International Journal of Precision Engineering and Manufacturing-Green Technology (2021) 8:405–421
https://doi.org/10.1007/s40684-020-00194-7
Online ISSN 2198-0810
Print ISSN 2288-6206

REGULAR PAPER

Cooling/Lubrication Performance of Dry and Supercritical CO_2-Based Minimum Quantity Lubrication in Peripheral Milling Ti-6Al-4V

Chongyan Cai[1] · Xu Liang[1] · Qinglong An[1] · Zhengrui Tao[1] · Weiwei Ming[1] · Ming Chen[1]

Received: 19 August 2019 / Revised: 7 November 2019 / Accepted: 20 January 2020 / Published online: 8 February 2020

Abstract
Cryogenic environments are often adopted in machining difficult-to-cut materials such as Ti-6Al-4V alloy to control its cutting heat and improve machinability. This paper aims to study the machinability of Ti-6Al-4V in finish milling process under four green cutting environments (CEs), i.e. dry, supercritical carbon dioxide (scCO_2), supercritical CO_2-based minimum quantity lubrication with water-based cutting fluid (scCO_2-WMQL), supercritical CO_2-based minimum quantity lubrication with oil-on-water droplets cutting fluid (scCO_2-OoWMQL). Peripheral finish-milling of Ti-6Al-4V was conducted under various cutting speeds, feed rates, radial depth of cut and CEs. The cutting force, cutting temperature, surface morphology and surface roughness were analysed. The experiment results show that the minimum cutting force and its coefficients, cutting temperature and surface roughness are obtained in scCO_2-OoWMQL environment because of its excellent cooling/lubrication and chip evacuation performance, whereas the worst friction in the tool-workpiece interface leads to the worst performance under scCO_2 CE. Additionally, the machined surface profile, cutting force and their spectrums under four CEs were studied. The fundamental frequency of machined surface profile is equal to that of cutting force envelope under dry and scCO_2 CEs, which is also called beat frequency, therefore scCO_2-WMQL and scCO_2-OoWMQL CEs can improve the milling stability. The results indicate that scCO_2-OoWMQL provides the best performance with regard to cutting force, cutting temperature, surface finish and clean production.

Keywords Supercritical CO_2 · Minimum quantity lubrication · Oil-on-water · Beat vibration · Cutting force coefficients · Peripheral milling

1 Introduction

Ti-6Al-4V alloy has many advantages such as high specific strength, good thermal strength, corrosion resistance and abundant resources. It has a wide range of applications in aerospace, defence industry and medical fields [1, 2]. However, the high chemical activity and the low thermal conductivity greatly affect the machinability of the titanium alloy [3]. In order to effectively control the rise of cutting temperature and cutting force, improve the friction state of the tool-work interface, suppress tool wear and improve the quality of the machined surface, it is necessary to apply cooling/lubrication conditions in machining Ti-6Al-4V.

✉ Qinglong An
qlan@sjtu.edu.cn

[1] School of Mechanical Engineering, Shanghai Jiao Tong University, Shanghai 200240, People's Republic of China

Although cutting fluids have been widely used in flood cooling system in manufacturing process, traditional cutting fluids also have their disadvantages, such as high cost, serious environmental pollution, difficulty in waste fluid treatment and threat to the health of operators. Amiril et al. [4] and Gajrani et al. [5] pointed out that in high productivity manufacturing enterprises, the cost of cutting fluid supply, maintenance and recycling together accounts for 17% of the manufacturing cost of the workpiece, while the cost of cutting tools only accounts for 2–4%. Moreover, the poor permeability of cutting fluid in flood cooling process often leads to lubricant film rupture and lubrication failure, due to the excessive temperature of the cutting zone [6]. Therefore, according to the requirements of environmental protection and sustainable development, it is necessary to improve and reduce the environmental pollution caused by cutting fluid, so as to realize cleaner production. Cleaner production requires green cutting technology in manufacturing process [7]. At present, green cutting technology can be divided into two categories: one is dry cutting technology without lubrications at all; the other is quasi-dry cutting technology, which requires a very small amount of cutting fluid that is degradable and harmless to the human body, such as steam cooling, liquid nitrogen cooling, MQL and cryogenic minimum quantity lubrication (CMQL). Although dry cutting can protect the environment and reduce costs to a large extent, the inevitable large cutting force and high cutting temperature in dry cutting will have an impact on the machinability. Complete dry cutting has a narrow range of applications due to the harsh requirements on cutting tools, process selection principles and other conditions. Quasi-dry combines the advantages of dry and flood cooling, which can not only meet the processing requirements, but also reduce the cost of cutting fluid to the lowest level and meet the same requirements as dry cutting [8, 9].

Yuan et al. [10] found that MQL condition cannot produce evident effect on cutting performance of Ti-6Al-4V, because oil mists cannot penetrate the contact layer to lubricate the cutting zone effectively due to the high temperature and load in tool-chip and tool-workpiece interfaces. Bordin et al. [9] pointed out that cryogenic semi-finish turning Ti-6Al-4V significantly reduces tool wear, improves surface finish and chip fragmentation compared with dry and wet cutting. Cryogenic machining is a sustainable manufacturing process for titanium alloy surgical prostheses. CMQL combines the efficient cooling of cryogenic machining with the lubrication effect of MQL, and solves the problem of insufficient cooling performance such as lubrication film breakdown caused by excessive temperature in cutting zone. CMQL technology has become a research hotspot of scholars.

There is extensive review on the application of MQL and CMQL techniques for machining titanium alloys [11]. Pereira et al. [11] optimized the CO_2 flow outlet diameter and velocity by utilizing computational fluid dynamics during CMQL machining and designed two nozzle adaptors to obtain best cooling/lubrication performance. Li et al. [2] pointed out that the addition of graphite nanoparticles in cutting fluid can significantly improve the cooling/lubrication performance of oil film in milling Ti-6Al-4V under MQL condition. Bai et al. [12] compared the cooling/lubrication performance of different nanofluids by dispersing Al_2O_3, SiO_2, MoS_2, CNTs, SiC, and graphite particles in cutting fluids, results showed that Al_2O_3 and SiO_2-based MQL obtained the lowest cutting force and surface roughness. Krolczyk et al. [7] found that compared with dry turning, the use of mineral oil-based cooling-lubricant can reduce the tool life by nearly 65% in duplex stainless turning process, they also found that when the cutting speed is high and the feed rate is small, the cutting force of dry turning is smaller than that under flood cooling condition, which means dry turning can achieve cleaner production for high cutting speed and low feed rate. Mia et al. [13] established a sustainability evaluation model under three sustainable processing technologies, i.e. dry cutting, MQL, solid lubrication system with compressed air cooling and traditional flood cooling by Pugh matrix environment method, results showed that MQL provides environment friendliness, cleaner production and helps to improve the desirable machinability characteristics. Krolczyk et al. [14] studied the parametric and non-parametric description of the machined surface after dry cutting and CMQL conditions. Results showed that the application of CMQL method can lead to the reduction of 3D surface roughness parameters compared to values reached after the dry machining, and the surface wear resistance was improved by CMQL. Bagherzadeh and Budak [15] proposed a new cooling technology in turning experiments of Ti-6Al-4V and Inconel 718 to improve the cooling effect of MQL and cryogenic CO_2, results showed that CMQL increase machinability and final product quality with low cooling rate consumption. Based on response surface methodology and Taguchi signal-to-noise ratio method, Mia [16] established a statistical model for the influence of feed rate, cutting speed and MQL flow rate on the cutting energy and surface roughness in end milling AISI 4140 steel. Behera et al. [17] studied the cutting force, tool wear, surface integrity and chip morphology of Inconel 718 under high-pressure jet, cryogenic, MQL and MQL with nanofluid CEs. They concluded that the cryogenic environment results in better surface integrity and reduced tool wear. Mia and Dhar [18] studied the cutting zone temperature, machinability of material and tool wear pattern by applying high-pressure coolant into tool-chip and tool-workpiece interfaces respectively. Results showed that high pressure coolant jet can significantly reduce cutting temperature, cutting force and surface roughness, and improve tool life. Faga et al. [19] investigated the process productivity and environmental impact in turning of Ti-6Al-4V under dry, MQL, emulsion mist and wet CEs. Wang et al. [6] proposed using cryogenic air with OoW droplets as an environmentally friendly cooling/lubrication method to reduce tool wear in turning compacted graphite cast iron. $scCO_2$-OoWMQL environment was also used in machining 316L stainless steel, under which the cutting force was reduced [20].

Although there are lots of studies on the performance of different cooling/lubrication conditions in machining hard-to-cut materials, the comprehensive analysis of machinability of Ti-6Al-4V peripheral finish-milling under sustainable green CEs, i.e. dry, $scCO_2$, $scCO_2$-WMQL, $scCO_2$-OoWMQL, is rarely reported. This paper investigates the cutting force and its coefficients, cutting temperature, surface morphology, surface roughness and milling stability under various cutting parameters and CEs. The mechanism of beat vibration in dry and $scCO_2$ CEs under specific cutting parameters is also studied, and the dependence of surface profile on milling force envelope is quantified. Finally, it is concluded that $scCO_2$-OoWMQL is the most suitable CE for the sustainability and green finish-milling of Ti-6Al-4V, and can promote cleaner production.

2 Experiment

2.1 Cooling/Lubrication Methods

Figure 1 shows the schematic diagram of the CMQL generator. The device has two separate oil-based and water-based cutting fluid storage tanks, two separate cutting fluid-air mixing chambers and two separate atomizing nozzles. Two different cutting fluids are transported to the mixing chamber through an oil pump, then atomized by high-pressure and high-speed air jet from the air compressor, and then entered the nozzle. Due to the expansion of oil molecules, they are adsorbed at the water-molecule interface, forming oil-on-water (OoW) droplets. Under the Joule–Thomson effect, the mixture of OoW droplets and air mixes with high-pressure, high-speed and normal-temperature CO_2 at the nozzle to form a cryogenic (approximately − 78℃) mixed jet of gaseous CO_2/solid-CO_2/ OoW droplets. It penetrates into the cutting zone at a high speed, resulting in a significant reduction in the temperature of the cutting zone and the surrounding environment for powerful cryogenic cooling and lubrication. Different cooling/lubrication methods, namely, $scCO_2$, $scCO_2$-WMQL and $scCO_2$-OoWMQL, can be obtained when controlling different valves. The diameter of the droplet particles is about 100 ~ 200 μm. The cooling/lubrication methods and their parameters are shown in Table 1.

2.2 Experiment Parameter

Figure 2a shows the photograph of experimental set-up. The peripheral milling was carried out on HURCO VMX42 three-axis vertical CNC machining centre with a positioning accuracy of 0.01 mm. The workpiece was Ti-6Al-4V alloy block with a shape of 50 × 50 × 20 mm and a hardness of 30-45HRC, and the chemical composition of Ti-6Al-4V is: Al 6.5%, V 4.25%, Fe 0.04%, C 0.02%, N 0.015%, O 0.16%, H 0.0018%, Ti, Bal [10]. The tool was a 4-edge cemented carbide end mill with a 1-4 μm diamond coating by CVD, a diameter of 6 mm, a blade length of 20 mm, a rake angle of

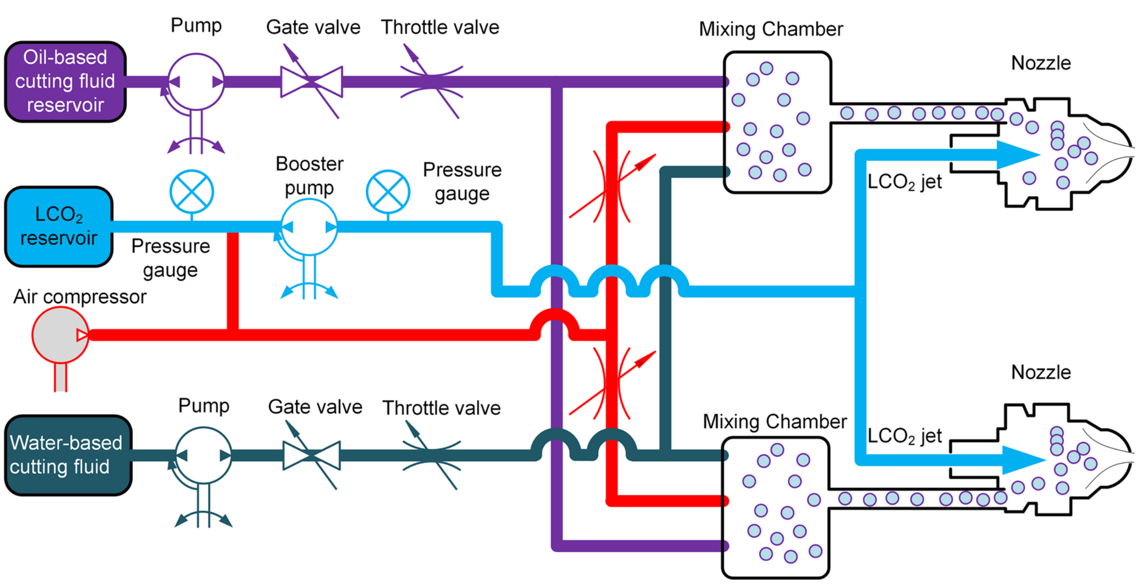

Fig. 1 Schematic diagram of CMQL generator

Table 1 Cooling/lubrication parameters

Environments	Cutting fluid and its operating parameters
Dry	–
$scCO_2$	Cutting fluid: liquid carbon dioxide, pressure: 7.5 bar
$scCO_2$-wMQL	Cutting fluid: antifreeze water-based cutting fluids (20% antifreeze water, 30% ethanol, 50% water), flow rate: 50 ml/h, pressure: 7.5 bar
$scCO_2$-OoWMQL	Cutting fluid: antifreeze water-based cutting fluids and soluble vegetable oil (1:1), flow rate: 50 ml/h, pressure: 7.5 bar

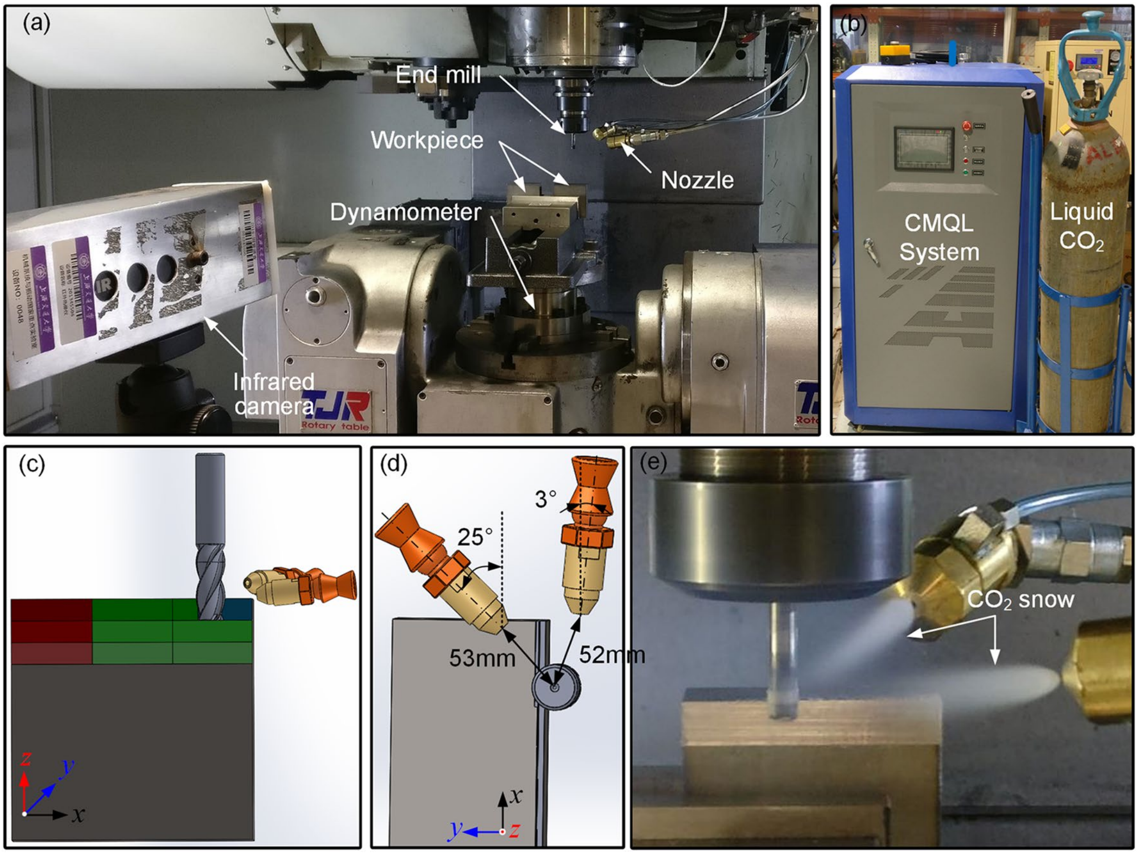

Fig. 2 **a** Experimental set-up **b** CMQL system **c** Nozzle arrangement diagram—main view **d** Nozzle arrangement diagram—top view **e** $scCO_2$ jet with lubricant particles

5° and a helix angle of 35°. The cutting force was measured by Kistler 9272 piezoelectric dynamometer, amplified by Kistler 5070A multi-channel charge amplifier and recorded by data acquisition card. The milling force acquisition frequency was 2 kHz. The milling temperature was measured using an infrared camera model FLIR A615, which has a resolution of 640 × 480 temperature points per frame and acquires 60 frames per second. The distance between infrared camera and cutting zone was 800 mm. An emissivity value of 0.5 was used for the Ti-6Al-4 V. The maximum cutting zone temperature at a machining length of 16.7 mm was taken as the characteristic temperature for each trial.

The temperature field in the cutting zone during milling is shown in Fig. 3. The atomizing nozzle with an inner diameter of 1.4 mm was mounted on the machining centre through a connecting plate, the gas/liquid two-phase CO_2 was delivered to the nozzle through a metal pipe having an inner diameter of about 5 mm, while the gas/liquid two-phase mixture of the cutting fluid droplets and air was delivered to the nozzle through a plastic pipe having an inner diameter of about 3 mm. Figure 2b shows the ARMORINE $scCO_2$-OoWMQL cooling/lubrication system and liquid CO_2 storage tank. As shown in Fig. 2c and d, distances between the centres of No. 1 and No. 2 nozzles to the tool centre are approximately 52 mm and 53 mm, respectively. Angles between the axes of No. 1 and No. 2 nozzles and the feed direction are 3° and 25°, respectively.

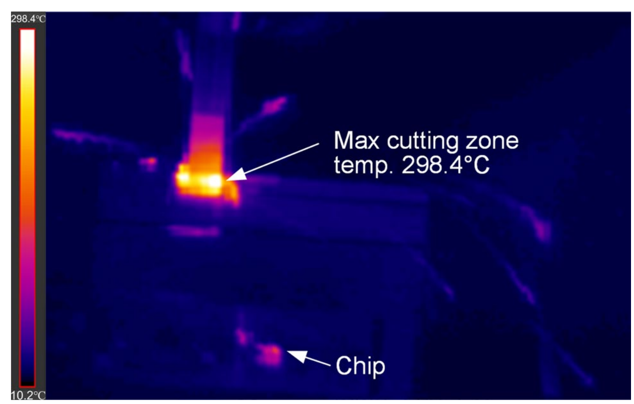

Fig. 3 Temperature field measured by infrared camera

Milling parameters are shown in Table 2. The cutting speed v_c, the feed per tooth f_z and the radial depth of cut a_e were single factor variables, each factor took three levels,

Table 2 Milling parameters

Experiment runs	Cutting speed v_c (m/min)	Feed per tooth f_z (mm/r)	Radial depth of cut a_e (mm)	Cooling/lubrication CEs	Tool
Nos. 1–3	20, 40, 60	0.045	0.3	Dry, $scCO_2$, $scCO_2$-WMQL, $scCO_2$-OoWMQL	1# 2# 3# 4#
Nos. 4–6	40	0.025, 0.035, 0.055	0.3		
Nos. 7–9	40	0.045	0.5, 0.7, 0.9		

and nine experiments under each CE were performed using one end mill. Three passes are performed under each milling parameter. The axial depth of cut of each pass is $a_p = 3$ mm, the machined surface length left under each parameter was 16.7 mm. The machining schematic is shown in Fig. 2c.

After the experiment, the machined surface morphology was taken using Keyence VHX-500 FE 3D microscopy system. The surface profile and roughness parameters were measured by Mitutoyo SJ-210 Portable Surface Roughness Tester based on the ISO 4288–1997 standards, the GAUSS filter was used with cut-off length $\lambda_c = 0.8$ mm and evaluation length $l_n = 5\ l = 4.0$ mm. During the measurement, the surface roughness was repeatedly measured 5 times on the machined surface of the first pass, and the average value was taken under each milling parameter.

3 Results and Discussion

3.1 Milling Force

During the down milling process, the thickness of the cutting layer is periodically reduced from maximum to zero, so the cutting force also changes periodically. The average resultant milling force over a period of time during the first pass is calculated by Eq. (1) under each cutting parameter and CE.

$$\overline{F} = \frac{\int_{t_1}^{t_2} \sqrt{F_x^2 + F_y^2 + F_z^2}\,dt}{t_2 - t_1} \tag{1}$$

where $\overline{F}$ is the average resultant milling force, F_x, F_y, F_z are the instantaneous milling force components in the feed x, normal y, and axial z direction, respectively, t_2 and t_1 are the upper and lower limits of the integral, respectively, and the integration time period is $t_2 - t_1 = 4$ s.

For each CE, the average reduction r of the cutting force relative to that under dry cutting condition is calculated by Eq. (2) [17].

$$r(\%) = \frac{1}{n}\sum_{i=1}^{n} r_i \tag{2}$$

where, r_i is the amount of reduction of the cutting force in the i-th test under $scCO_2$, $scCO_2$-WMQL and $scCO_2$-OoWMQL with respect to that under dry cutting, and n represents the number of tests.

For $v_c = 40$ m/min, $a_e = 0.3$ mm and $a_p = 3$ mm, the variation of cutting force with feed rate under each CE is shown in Fig. 4a, and the changes of cutting force in different cooling/lubrication environments relative to that in dry cutting environment are shown in Fig. 4b. The cutting force increases with increasing feed rate regardless of CEs, which is also observed by Behera et al. [17]. and Mia [21]. This rise can be attributed to the increased cutting layer area for higher feed rate. The order of cutting force under different CEs is $scCO_2$ > dry > $scCO_2$-WMQL > $scCO_2$-OoWMQL. The average changes of cutting force under $scCO_2$, $scCO_2$-WMQL, $scCO_2$-OoWMQL CEs with respect to that under dry cutting are 49.0%, -20.4% and -28%, respectively. Surprisingly, the utilization of $scCO_2$ condition significantly increases the cutting force. In particular, when feed

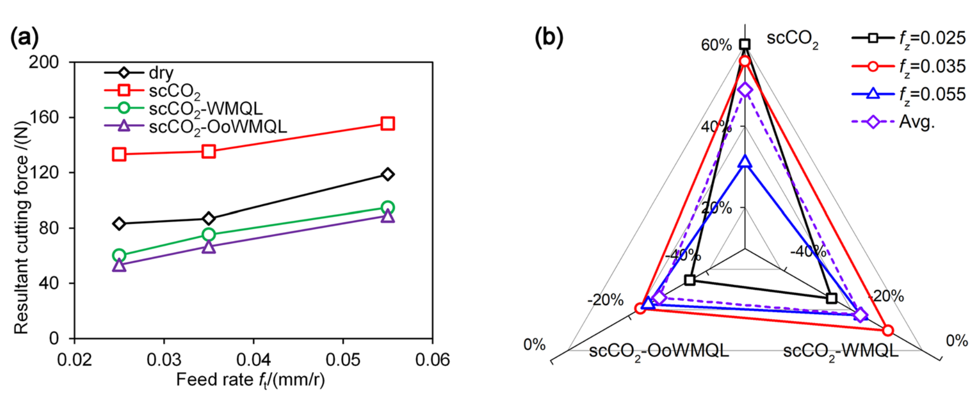

Fig. 4 **a** Cutting force vs. feed rate **b** Percentage changes of cutting force under cooling/lubrication environments relative to that under dry cutting

rate is very small ($f_z = 0.025$ mm/min), the cutting force increases by 60.1%. This can be attributed to the fact that the strength and hardness of Ti-6Al-4V alloys increase with the decrease of temperature [22], under $scCO_2$ condition, the cutting deformation resistance increases, and the friction in tool-workpiece interface deteriorates. However, when cutting fluid is mixed into cryogenic CO_2, the cutting forces decrease significantly relative to dry cutting. Particularly, for small feed rate ($f_z = 0.025$ mm/min), the reductions of cutting forces of $scCO_2$-WMQL and $scCO_2$-OoWMQL are the largest with respect to dry cutting, which are − 27.7%, − 35.9%, respectively. Although the cryogenic environment increases the strength of the workpiece material, high speed liquid CO_2 and lubricant jets can lift the chip and reduce the contact length between chip and tool rake face, and the presence of lubricant reduces the friction coefficients of tool-chip and tool-workpiece interfaces, so in view of this, the cutting forces of $scCO_2$-WMQL and $scCO_2$-OoWMQL are still reduced relative to that of dry cutting. The cutting force of $scCO_2$-OoWMQL is smaller than that of $scCO_2$-WMQL, which can be ascribed to the larger viscosity and better lubricating performance of OoW droplets than those of water droplets.

For $f_z = 0.045$ mm/rev, $a_e = 0.3$ mm and $a_p = 3$ mm, the variation of cutting force with v_c under each CE is shown in Fig. 5a, and the changes of cutting force in different cooling/lubrication environments relative to that in dry cutting are shown in Fig. 5b. The cutting force increases as v_c increases regardless of CEs, which is also observed by Korkut and Donertas [23]. In different cutting speed ranges, the variation trend of cutting force with cutting speed is different. The cutting force decreases with the increase of cutting speed for high speed. Because when v_c increases, the chip flow speed increases, and the friction coefficients of tool-chip and tool-workpiece interfaces decrease [7, 17, 18], the temperature in the cutting zone increases, which softens the material and make it easier to be removed [18, 23, 24], the chips become thinner and the cutting thickness decreases [17, 25]. However, the cutting speed of this experiment is low enough to produce sufficient cutting temperature to soften the material. Moreover, the built-up edge (BUE) is prone to be induced for low v_c range, the BUE first reaches a peak followed by a decrease with the increase of v_c [23]. As the v_c increases, the built-up edge dissipates and the actual rake angle γ_o decreases, resulting in an increase in cutting force. As shown in Fig. 5b, for intermediate cutting speed ($v_c = 60$ m/min), the changes of cutting forces of $scCO_2$, $scCO_2$-WMQL and $scCO_2$-OoWMQL with respect to dry cutting are 8.0%, − 3.4% and − 20.8%, respectively, whereas they are 22.8%, 19.7% and − 10.3% respectively for low cutting speed ($v_c = 40$ m/min). This means that the application of cooling/lubrication CE increases the cutting force (the reduction in cutting force is reduced for $scCO_2$-OoWMQL due to its best lubrication performance), which is precisely because cooling/lubrication CEs inhibit the generation of BUE then reduce the actual rake angle, resulting in a higher cutting force compared to dry cutting.

As shown in Fig. 6a, for $f_z = 0.045$ mm/rev, $v_c = 40$ m/min and $a_p = 3$ mm, the cutting force increases with radial cutting depth a_e regardless of CEs. It can be accredited to the increased cutting layer thickness per rotation cycle of tool for higher a_e. The order of cutting force under different CEs is $scCO_2$ > dry > $scCO_2$-WMQL > $scCO_2$-OoWMQL. Correspondingly, the average percentage changes compared to dry cutting are 37.8%, 0, − 0.9%, − 18.8%, − 27.0%, respectively. It can be seen from Fig. 6b that as a_e increases, the percentage change in cutting force decreases because the tool-workpiece contact time per rotation cycle increases and the cooling/lubrication effect is reduced.

It can be concluded that under different CEs, $scCO_2$-OoWMQL is the best way to reduce cutting force due to its best cooling/lubrication performance, whereas simply using cryogenic CE ($scCO_2$) will increase the cutting force. $scCO_2$-OoWMQL CE can also promote chip cleaning and inhibit formation of BUE.

3.2 Milling Force Coefficients

The force diagram of the milling cutter is shown in Fig. 7. The total milling force can be decomposed into the plough

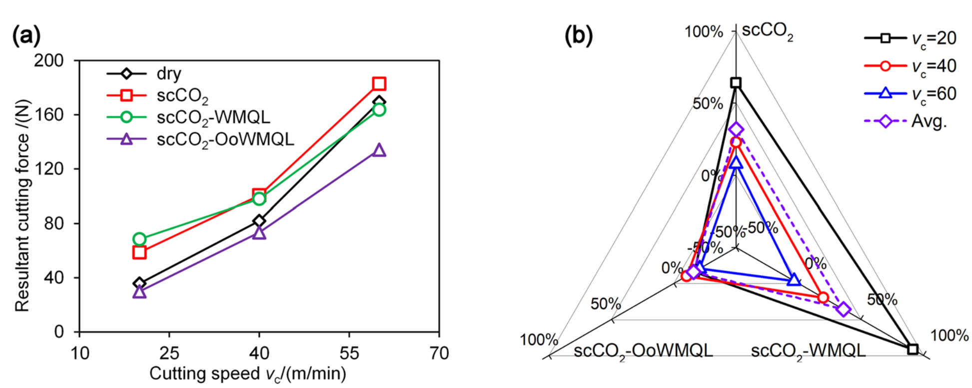

Fig. 5 **a** Cutting force vs. cutting speed **b** Percentage changes of cutting force under cooling/lubrication environments relative to that under dry cutting

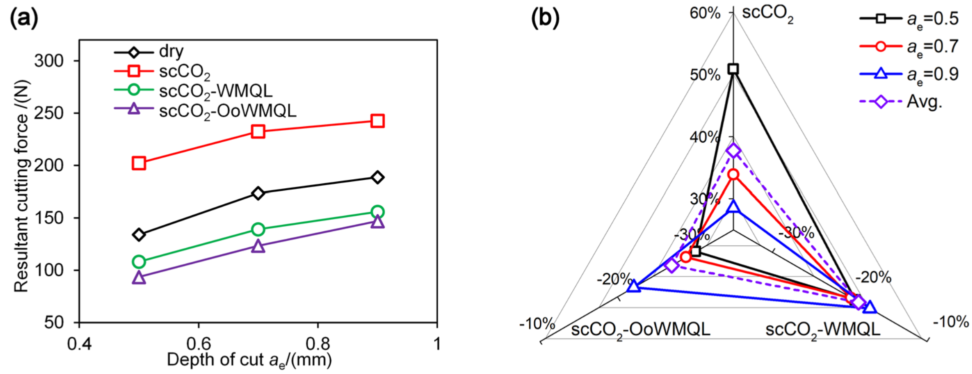

Fig. 6 **a** Cutting force vs. radial depth of cut **b** Percentage changes of cutting force under cooling/lubrication environments relative to that under dry cutting

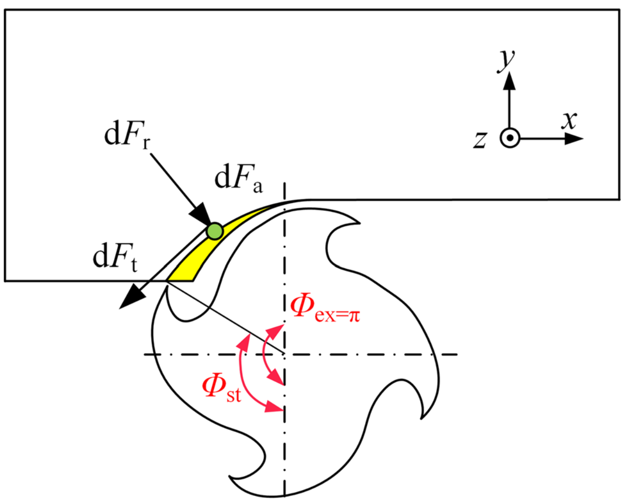

Fig. 7 The force diagram of the milling cutter

force component and the cutting force component. The plough force is generated by the existence of the blunt radius of tool edge and the friction between tool and workpiece, and the cutting force is generated due to shear deformation of the material [26]. The differential milling forces in the tangential, dF_t, radial, dF_r, and axial, dF_a, directions are shown in Eq. (3) [27].

$$
\begin{aligned}
dF_{tj}(\Phi, z) &= \left[K_{te} + K_{tc}h_j(\Phi, z)\right]dz \\
dF_{rj}(\Phi, z) &= \left[K_{re} + K_{rc}h_j(\Phi, z)\right]dz \\
dF_{aj}(\Phi, z) &= \left[K_{ae} + K_{ac}h_j(\Phi, z)\right]dz
\end{aligned}
\tag{3}
$$

where, Φ is tool immersion angel, z is the axial height of a point of the tooth, j is the tooth number. K_{te}, K_{re} and K_{ae} are tangential, radial and axial plough force coefficients, respectively, which relate the total cutting force and the ploughing and friction effect of cutting edge. K_{tc}, K_{rc}, and K_{ac} are the tangential, radial, and axial cutting force coefficients, respectively, which relate the total cutting force and shearing action of the cutting layer [28].

The milling force components in feed direction x, F_x, normal direction y, F_y, axial direction z, F_z can be expressed as a function of F_t, F_r and F_a.

$$
\begin{pmatrix} F_x \\ F_y \\ F_z \end{pmatrix} = \begin{pmatrix} \cos\Phi & \sin\Phi & 0 \\ -\sin\Phi & \cos\Phi & 0 \\ 0 & 0 & 1 \end{pmatrix} \begin{pmatrix} F_t \\ F_r \\ F_a \end{pmatrix}
\tag{4}
$$

The cutting force data of the first pass is used to calculate the milling force coefficient to avoid the ploughing and friction effect of the tool on the previous machined surface during the second and third passes. According to the method proposed by Budak [28], the milling force coefficients are calculated by Eq. (5).

$$
\begin{aligned}
K_{te} &= -\frac{\overline{F}_{xe}\frac{aN}{2\pi}[\sin\phi]_{\phi_{st}}^{\phi_{ex}} + \overline{F}_{ye}\frac{aN}{2\pi}[\cos\phi]_{\phi_{st}}^{\phi_{ex}}}{\left(\frac{aN}{2\pi}[\sin\phi]_{\phi_{st}}^{\phi_{ex}}\right)^2 + \left(\frac{aN}{2\pi}[\cos\phi]_{\phi_{st}}^{\phi_{ex}}\right)^2} \\
K_{tc} &= 4\frac{\overline{F}_{xc}\frac{aN}{2\pi}[\cos 2\phi]_{\phi_{st}}^{\phi_{ex}} + \overline{F}_{yc}\frac{aN}{2\pi}[2\phi - \sin 2\phi]_{\phi_{st}}^{\phi_{ex}}}{\left(\frac{aN}{2\pi}[\cos 2\phi]_{\phi_{st}}^{\phi_{ex}}\right)^2 + \left(\frac{aN}{2\pi}[2\phi - \sin 2\phi]_{\phi_{st}}^{\phi_{ex}}\right)^2} \\
K_{re} &= -\frac{K_{te}\frac{aN}{2\pi}[\sin\phi]_{\phi_{st}}^{\phi_{ex}} + \overline{F}_{xe}}{\frac{aN}{2\pi}[\cos\phi]_{\phi_{st}}^{\phi_{ex}}} \\
K_{rc} &= \frac{K_{tc}\frac{aN}{2\pi}[\cos 2\phi]_{\phi_{st}}^{\phi_{ex}} - 4\overline{F}_{xc}}{\frac{aN}{2\pi}[2\phi - \sin 2\phi]_{\phi_{st}}^{\phi_{ex}}}
\end{aligned}
\tag{5}
$$

where, Φ_{ex} is the tool cut-out angle, Φ_{st} is the tool cut-in angle, for down milling, $\Phi_{ex} = \pi$ and $\Phi_{st} = \pi - \cos^{-1}(1 - a_e/R)$. a is axial depth of cut, N is the number of teeth. F_{xe}, F_{ye}, F_{xc}, F_{yc} are the algebraic mean of cutting forces, which can be fitted by Eq. (6). The correlation coefficients R^2 of the fitting under four CEs are shown in Fig. 8. R^2 is very close to 1 in each CE, indicating that the fitting results are reliable.

$$
\overline{F}_q = \overline{F}_{qe} + f_z\overline{F}_{qc} \quad (q = x, y)
\tag{6}
$$

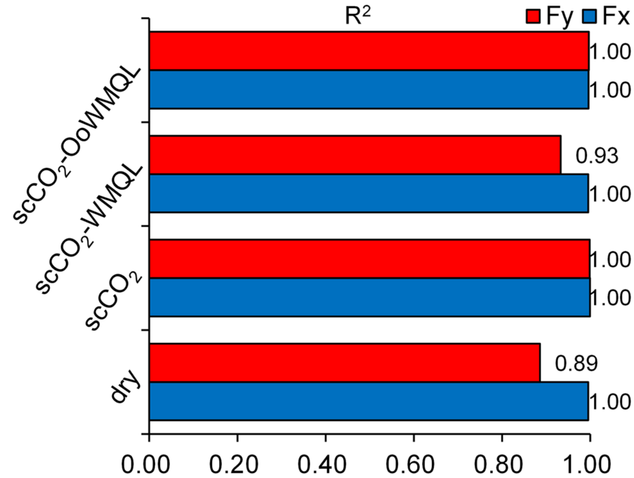

Fig. 8 Correlation coefficients R^2 of the fitting

The edge force coefficients and the cutting force coefficients under four CEs are shown in Fig. 9a, b respectively. For edge force coefficients, K_{re} is always greater than K_{te} regardless of CE, particularly in $scCO_2$ CE, K_{re} is 350% larger than K_{te}. This is because the spring-back phenomenon in machining Ti-6Ak-4V is very serious. The rankings of K_{te} and K_{re} under different CEs are $scCO_2$ > dry > $scCO_2$-WMQL > $scCO_2$-OoWMQL which is identical with the ranking of cutting force (Figs. 4, 5 and 6), therefore, it can be inferred that ploughing force accounts for a large part of total cutting force. K_{te} and K_{re} can represent the friction between the tool-workpiece and the tool-chip interfaces. In $scCO_2$ CE, K_{te} and K_{re} increases by 31.3% and 113.0%, respectively, compared to those under dry CE, which indicates that the friction between tool and workpiece/chip is deteriorated under $scCO_2$ CE during finish-milling of Ti-6Al-4V, and accounts for the increased cutting force under $scCO_2$ CE compared to dry CE (Figs. 4, 5 and 6). After the addition of lubricants to $scCO_2$ jet, the friction is greatly improved. In $scCO_2$-OoWMQL CE, K_{te} and K_{re} are reduced by − 49.5% and − 39.4%, respectively, relative to those under dry cutting. The reduction of K_{te} and K_{re} in $scCO_2$-OoWMQL are larger than those in $scCO_2$-WMQL (− 42.4% and − 3.6%, respectively), it can be ascribed to fact that the OoW droplet has a higher viscosity than water, and the tool-workpiece interface is easier to form a lubricating film, which is beneficial to reduce the friction.

It can be seen from Fig. 9b that K_{rc} is less than K_{tc} in the three cooling/lubricating environments, which is different from dry cutting. The tangential cutting force coefficient does not change much in the cooling/lubrication environment. For $scCO_2$ CE, K_{tc} is slightly increased by 1.8% compared with dry cutting, and only reduced by − 4.7% and − 13.2% respectively in $scCO_2$-WMQL and $scCO_2$-OoWMQL CEs, which indicates that the effect of cooling/lubrication on shear of cutting layer is not significant. However, the radial cutting force coefficients are greatly reduced by − 28.5%, − 40.5% and − 43.5% under $scCO_2$, $scCO_2$-WMQL and $scCO_2$-OoWMQL CEs, respectively, which suggests that the application of cooling/lubrication reduces the spring-back of Ti-6Al-4V in milling process.

3.3 Cutting Temperature

The average value of the maximum cutting temperature $\overline{T}_{CE}$ for different CEs is calculated by Eq. (7).

$$\overline{T}_{CE} = \frac{1}{n}\sum_{i=1}^{n}\overline{T}_{CE\_i} \tag{7}$$

where, CE is cutting environment, $\overline{T}_{CE\_i}$ represents the maximum cutting temperature measured under the i-th trial in specific CE, and n represents the number of tests. The effect of cutting parameters on cutting temperature under different CEs is shown in Fig. 10.

For $f_z = 0.045$ mm/rev, $a_e = 0.3$ mm and $a_p = 3$ mm, the variation of cutting temperature with v_c under each CE is

Fig. 9 **a** Edge force coefficients and **b** Cutting force coefficients under different CEs

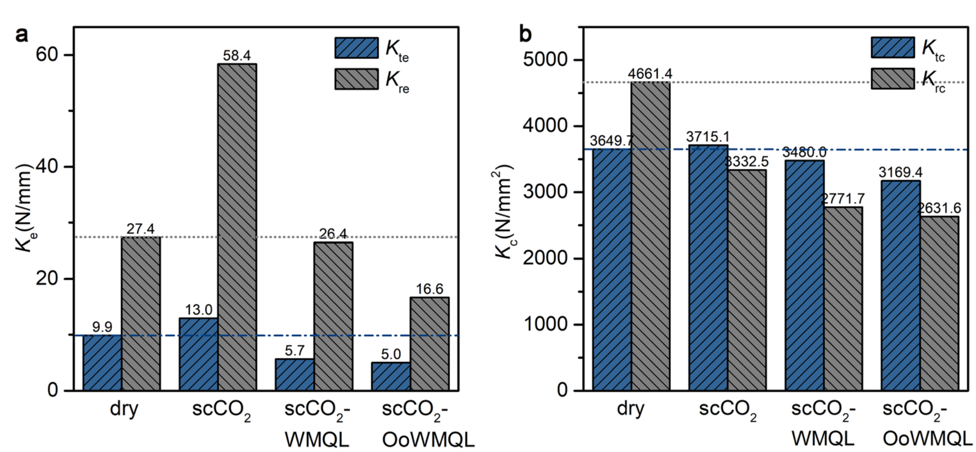

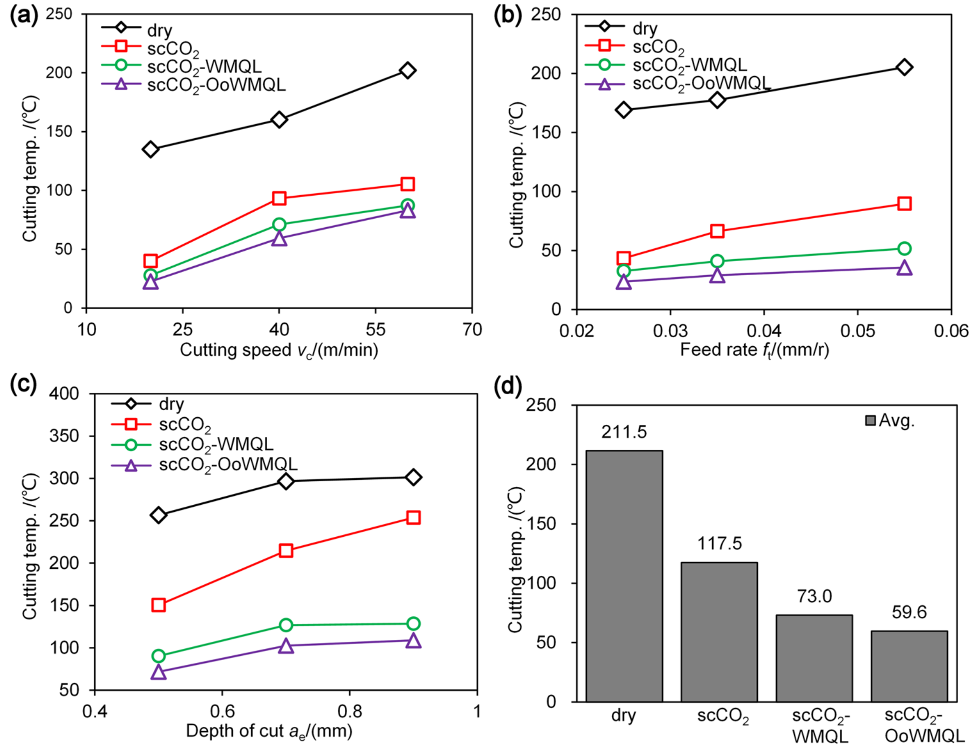

Fig. 10 Cutting temperature vs. **a** cutting speed **b** feed rate **c** radial depth of cut **d** cutting environments

shown in Fig. 10a. The cutting temperature increases with increasing v_c regardless of CEs, because the amount of metal removal per unit time, the work done by tool and the heat generated by shear and friction increase with the increase of v_c. As shown in Fig. 10b, c, the cutting temperature increases with increasing f_z or a_e regardless of CEs, the increased material removal and heat generated in the cutting zone for higher f_z or a_e account for this phenomenon. However, the increase in cutting temperature with the increase in f_z or a_e is not as significant as v_c. This can be attributed to the fact that although the heat generation per unit time increases as f_z or a_e increases, the tool-chip contact length also increases, and the heat dissipation improves. Due to the application of $scCO_2$ and lubricants, the cutting temperatures under $scCO_2$-WMQL and $scCO_2$-OoWMQL change slower with cutting parameters compared to dry cutting.

As shown in Fig. 10d, the cutting temperature under different CEs in descending order is: dry > $scCO_2$ > $scCO_2$-WMQL > $scCO_2$-OoWMQL. $scCO_2$ significantly reduces the cutting temperature, which is 44.4% lower than dry cutting. Four reasons accounts for this: (1) High-pressure high-speed cryogenic $scCO_2$ jet realizes forced convection heat transfer. (2) After the $scCO_2$ droplets are sprayed into the cutting zone, the droplets undergo vaporization, taking away part of the cutting heat. (3) The use of $scCO_2$ jet can promote chip evacuation, thereby promoting the release of cutting heat from chips. (4) $scCO_2$ jet can even cause chip breaking or chip lifting, reducing contact length between chip and rake face, thereby reducing friction heat.

By adding a minimum quantity of lubricant to $scCO_2$, the cutting temperature is further reduced. As shown in Fig. 10d, the cutting temperatures in the $scCO_2$-WMQL and $scCO_2$-OoWMQL are further reduced by 37.9% and 49.3%, respectively, relative to the temperature in the $scCO_2$ environment. This is because the lubricants in $scCO_2$-WMQL and $scCO_2$-OoWMQL CEs reduce the friction coefficients between tool-chip and tool-workpiece interfaces, resulting in lower cutting force then friction heat, and the vaporization of the lubricant particles also carry away a part of the heat. $scCO_2$-OoWMQL shows better performance with regard to cutting temperature than $scCO_2$-WMQL, this can be accredited to the higher viscosity of OoW particles than that of water molecules, making it easier to form a lubricating film in the cutting zone.

3.4 Surface Roughness

The average value of the surface roughness $\overline{Ra}_{CE}$ for different CEs is calculated by Eq. (8).

$$\overline{Ra}_{CE} = \frac{1}{n}\sum_{i=1}^{n}\overline{Ra}_{CE\_i} \tag{8}$$

where, $\overline{Ra}_{CE\_i}$ represents the surface roughness measured under the i-th trial in specific CE. The effect of cutting parameters on surface roughness under different CEs is shown in Fig. 11.

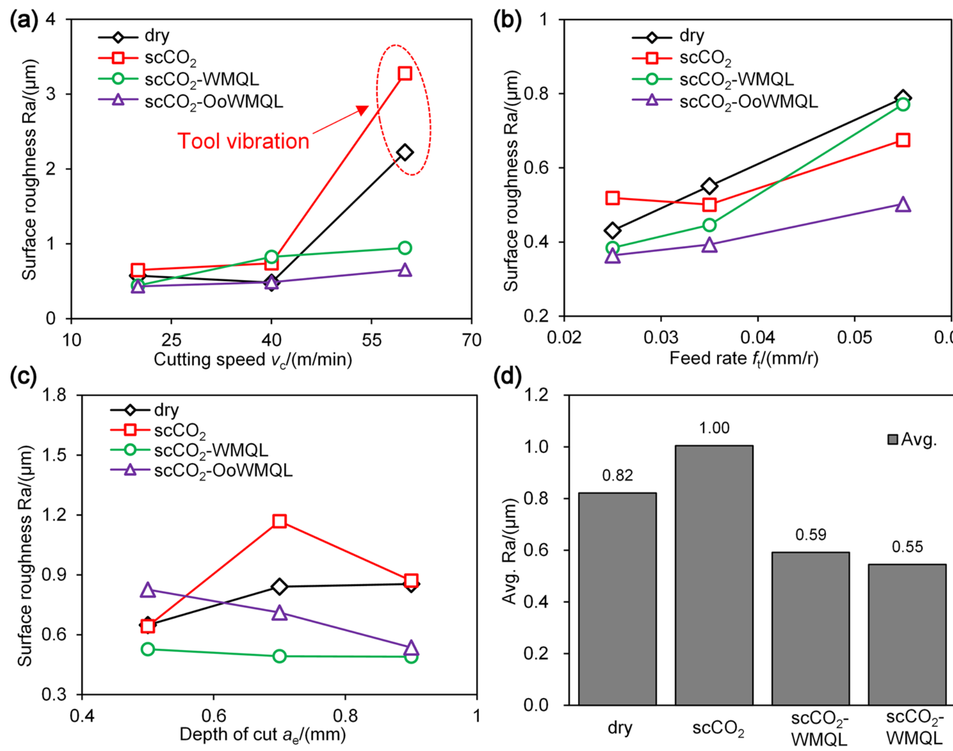

Fig. 11 Surface roughness vs. **a** cutting speed **b** feed rate **c** radial depth of cut **d** cutting environments

As shown in Fig. 11a, for $f_z = 0.045$ mm/rev, $a_e = 0.3$ mm and $a_p = 3$ mm, the surface roughness increases with increasing v_c regardless of CEs, this is because the cutting force and the cutting temperature also increase for higher cutting speed, resulting in worse surface quality. It can be found from Fig. 11a that when the cutting speed is $v_c = 60$ m/min, the surface roughness is 2.22 μm and 3.28 μm in dry and $scCO_2$ CEs, respectively, which is much larger than that in the $scCO_2$-WMQL and $scCO_2$-OoWMQL CEs (0.95 μm and 0.65 μm, respectively). Observation of the machined surface shows that beat vibration of tool occurs, which will be discussed in more detail in Sect. 3.4. As shown in Fig. 11b, for $v_c = 40$ m/min, $a_e = 0.3$ mm and $a_p = 3$ mm, the surface roughness increases with feed rate regardless of CEs, which can be attributed to the higher theoretical residual contour for the increased feed rate. As shown in Fig. 11c, radial depth of cut has little effect on surface roughness, which is also observed by Mia et al. [13].

There is a certain error in measuring the surface roughness using the probe type roughness measuring instrument, and the surface roughness difference is small under different CEs during finish-milling process. So the average surface roughness of nine experiments under each CEs will be used to compare the influence of CE on surface roughness. As shown in Fig. 11d, the surface roughness R_a is in the range of 0.55–1.0 μm, R_a under different CEs in descending order is $scCO_2 >$ dry $> scCO_2$-WMQL $> scCO_2$-OoWMQL, which is consistent with ranking of the edge force coefficients under four CEs (Fig. 9a). This indicates that friction property is a direct factor affecting R_a in different CEs. Surprisingly, although $scCO_2$ jet promotes chip evacuation and cleans chippings on the tool and machined surface, R_a of $scCO_2$ CE is still 22% greater than that of dry cutting. This is because the edge force coefficients of $scCO_2$ are the largest, which indicates that the friction between tool and workpiece deteriorates. R_a in $scCO_2$-WMQL and $scCO_2$-OoWMQL CEs is less than that in $scCO_2$ CE, because water molecules and OoW particles improve the lubrication of tool-workpiece interface. The better lubrication performance of OoW particle is accredited with the better surface finish of $scCO_2$-OoWMQL than that of $scCO_2$-WMQL.

3.5 Beat Vibration

When $v_c = 60$ m/min, $f_z = 0.045$ mm/r, $a_e = 0.3$ mm (Experiment No. 3), the machined surface topography of four CEs is shown in Fig. 12 (The machined surface magnified 20 times is in the left side and that of the third tool path magnified 200 times is in the right side). The surface waviness caused by tool vibration is clearly observed in dry and $scCO_2$ CEs, but not found in $scCO_2$-WMQL and $scCO_2$-OoWMQL CEs. The direction of the surface waviness is along the tool axis, perpendicular to the feed direction. The direction of the surface waviness is consistent after three passes of tool, which indicates that the deflection and vibration of tool are most severe during the third pass of tool, covering the ripples generated during the first and second passes. Only abrasive sliding grooves parallel to the direction of cutting speed and

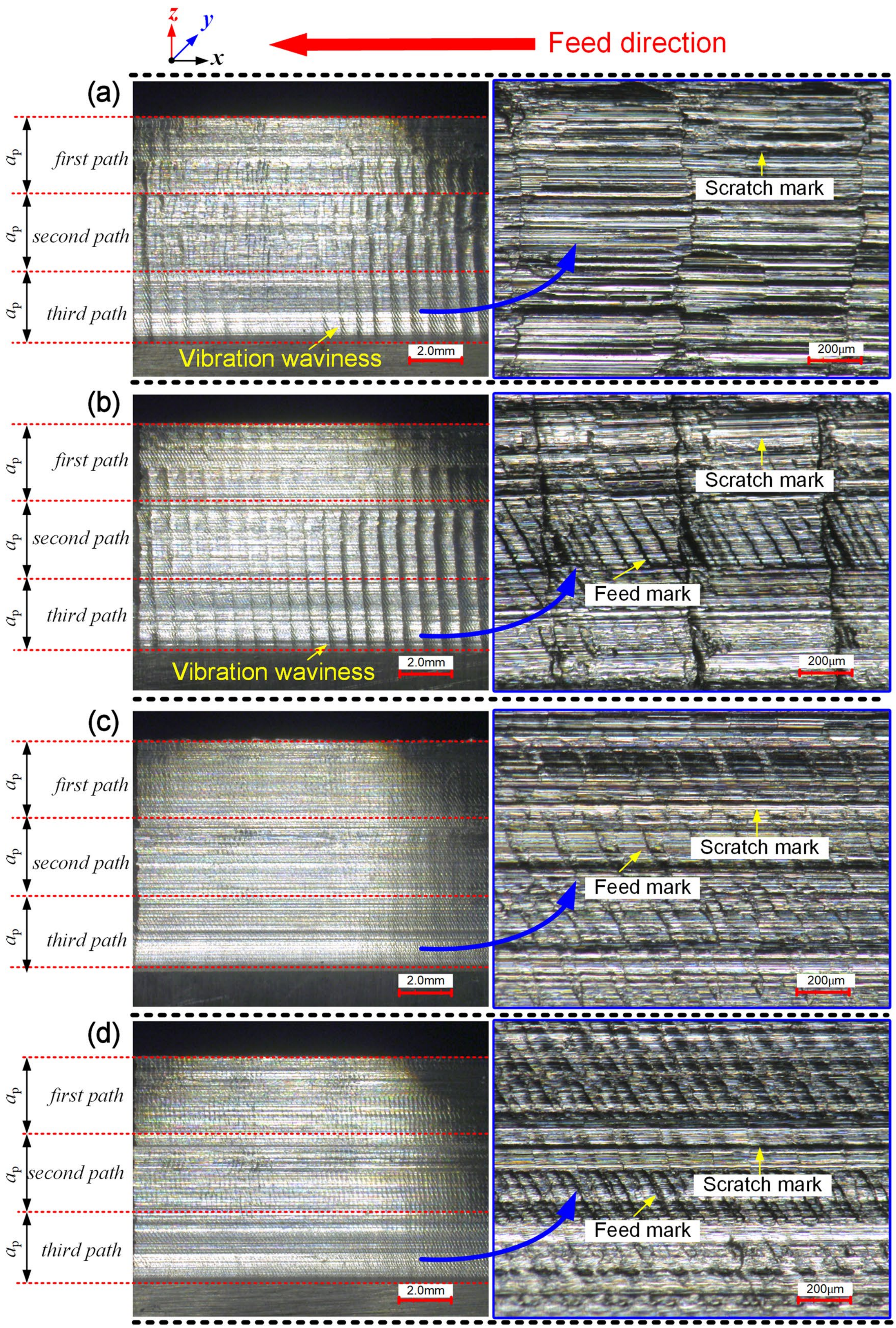

Fig. 12 Machined surface topography of experiment No. 3 **a** dry **b** $scCO_2$ **c** $scCO_2$-WMQL **d** $scCO_2$-OoWMQL

feed marks are observed on the machined surfaces under $scCO_2$-WMQL and $scCO_2$-OoWMQL CEs.

The machined surface profile and its spectrum of the third tool pass of experiment No. 3 are shown in Fig. 13. When only the relative motion of tool and workpiece is considered, the machined surface topography is only a copy of the tool geometry. Theoretically, the distance between adjacent peaks of surface profile is $f_z = 45$ μm,

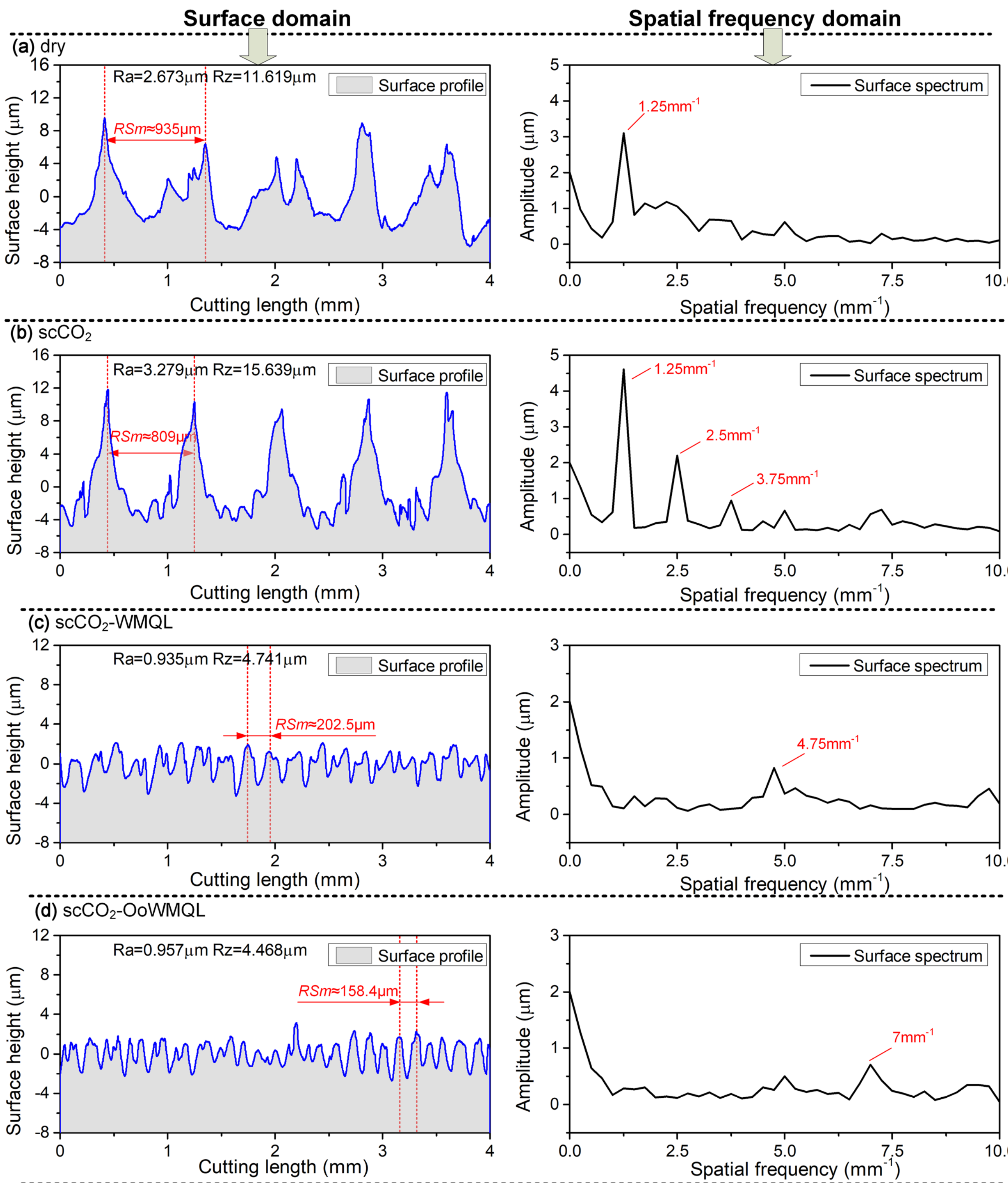

Fig. 13 Machined surface profile and its spectrum of experiment No. 3 **a** dry **b** $scCO_2$ **c** $scCO_2$-WMQL **d** $scCO_2$-OoWMQL

however, the mean width of the profile elements *RSm* under four CEs is greater than f_z, which is 935, 809, 202.5 and 158.4 μm, respectively. This is because the tool-workpiece system will vibrate during milling process, which has a much greater effect on the surface topography than the effect of feed on that. *RSm* under different CEs in descending order is dry > $scCO_2$ > $scCO_2$-WMQL > $scCO_2$-OoWMQL, which is identical with the order of cutting force (Fig. 5a), indicating that cutting force has a great influence on surface morphology. The *RSm* values of $scCO_2$-WMQL and $scCO_2$-OoWMQL are 202.5 and 158.4 μm, respectively, which are approximately four times of f_z, namely the feed length in a tool rotation cycle. The manufacturing error or radial run-out of the tool is accredited with this phenomenon. However, under dry and $scCO_2$ CEs, the *RSm* values are 935 and 809 μm respectively, which are approximately 20 times of f_z, indicating that the tool is significantly vibrating during milling process.

The vibration of tool under dry and $scCO_2$ CEs can be confirmed from the spectrum of surface profile in the spatial frequency domain, which is obtained by the Fast Fourier Transform (FFT) and shown in Fig. 13. Theoretically, the spectrum of machined surface profile in the spatial frequency domain consists of the tooth passing frequency s_{tp} due to feed and the spindle frequency s_{sp} due to manufacturing error or radial run-out of tool. According to the octave property, the spectrum will appear at the fundamental frequency and its integer multiple, as shown in Eq. (9).

$$\begin{cases} s_{tp} = \frac{k}{f_z}, \quad k = 1,\ 2,\ 3.... \\ s_{sp} = \frac{k}{zf_z}, \quad k = 1,\ 2,\ 3.... \end{cases} \tag{9}$$

where, z is the number of teeth, in this experiment $z=4$. k is a positive integer, which represents the fundamental frequency when $k=1$, and represents the frequency multiplication when $k=2, 3, 4....$ When $v_c=60$ m/min, $f_z=0.045$ mm/r, $a_e=0.3$ mm (Experiment No. 3), the fundamental frequency of s_{tp} and s_{sp} in the spatial domain are 22.2 mm^{-1} and 5.55 mm^{-1}, respectively.

In accordance with expectations, the tooth passing frequency s_{tp} and spindle frequency s_{sp} in spatial domain are not observed in the spectrum of dry and $scCO_2$ CEs due to tool vibration. The spectrum of surface profile moves to low frequency band obviously in dry and $scCO_2$ CEs compared with that in $scCO_2$-WMQL and $scCO_2$-OoWMQL CEs, which means an increase in the peak-to-peak distance of the surface profile. The main frequency of surface profile in the $scCO_2$-WMQL and $scCO_2$-OoWMQL environments is only close to s_{sp} (5.55 mm^{-1}), which is 4.75 mm^{-1} and 7 mm^{-1}, respectively. This phenomenon may be ascribed to lateral flow of materials during milling process, Nieslony et al. [29] pointed out that it may also be due to errors of probe surface profilometer.

The tooth pass frequency f_{tp} and spindle frequency f_{sp} in the time domain are calculated by Eq. (10).

$$\begin{cases} f_{tp} = \frac{knz}{60}, \quad k = 1,\ 2,\ 3.... \\ f_{sp} = \frac{kn}{60_z}, \quad k = 1,\ 2,\ 3.... \end{cases} \tag{10}$$

where n is spindle speed in r/min, which is calculated by Eq. (11). Under experiment No. 3, $n=3183$r/min and $f_{tp}=212.21$ Hz are obtained.

$$v_c = \frac{\pi dn}{1000} \tag{11}$$

When the vibration frequency f_c of the tool in the time domain is less than $f_{tp}/2$, vibration waviness will be generated on machined surfaces [30].

$$y_t(x) = \sum_{n=0}^{\infty} a_n(A) \sin\left(2\pi n \frac{f_c}{f_z f_{tp}} x\right) \tag{12}$$

where, A is the vibration amplitude of the tool in normal direction, $f_c/(f_z{*}f_{tp})$ is the fundamental frequency of machined surface profile in spatial domain. Therefore, it can be determined that the vibration frequency f_c of tool is 11.94 Hz in dry and $scCO_2$ CEs, as shown in Eq. (13).

$$f_c = f_z f_{tp} \times 1.25 = 11.94\boldsymbol{Hz} \tag{13}$$

The octave of machined surface spectrum under $scCO_2$ CE proves that tool vibration does occur, although the machine surface spectrum of dry CE does not exhibit octave property, which is because chips scratch or adhere to the machined surface due to bad chip evacuation performance of dry CE, causing the waviness generated by tool vibration to be destroyed.

In order to analyse the cause of surface waviness of dry and $scCO_2$ CEs under experiment No. 3 ($v_c=60$ m/min, $f_z=0.045$ mm/r, $a_e=0.3$ mm), it is necessary to investigate the milling force characteristics. For experiment No. 3, the dynamic milling force in normal direction (F_y) and its envelops varying with cutting length under each CE is shown in Fig. 14. The spectrums of F_y and its upper envelop are also obtained by FFT as shown in Fig. 14. Under dry and $scCO_2$ CEs, the amplitude of F_y varies periodically and slowly with cutting length (the upper and lower envelopes of F_y are shown in the figure), as if the amplitude of high-frequency tooth passing signal is modulated by the low-frequency carrier signal, which indicates that the beat vibration of tool-workpiece system occurs during milling process. Beat vibration occurs when there are two sources of vibration at closely spaced frequencies and amplitudes, which can be verified by

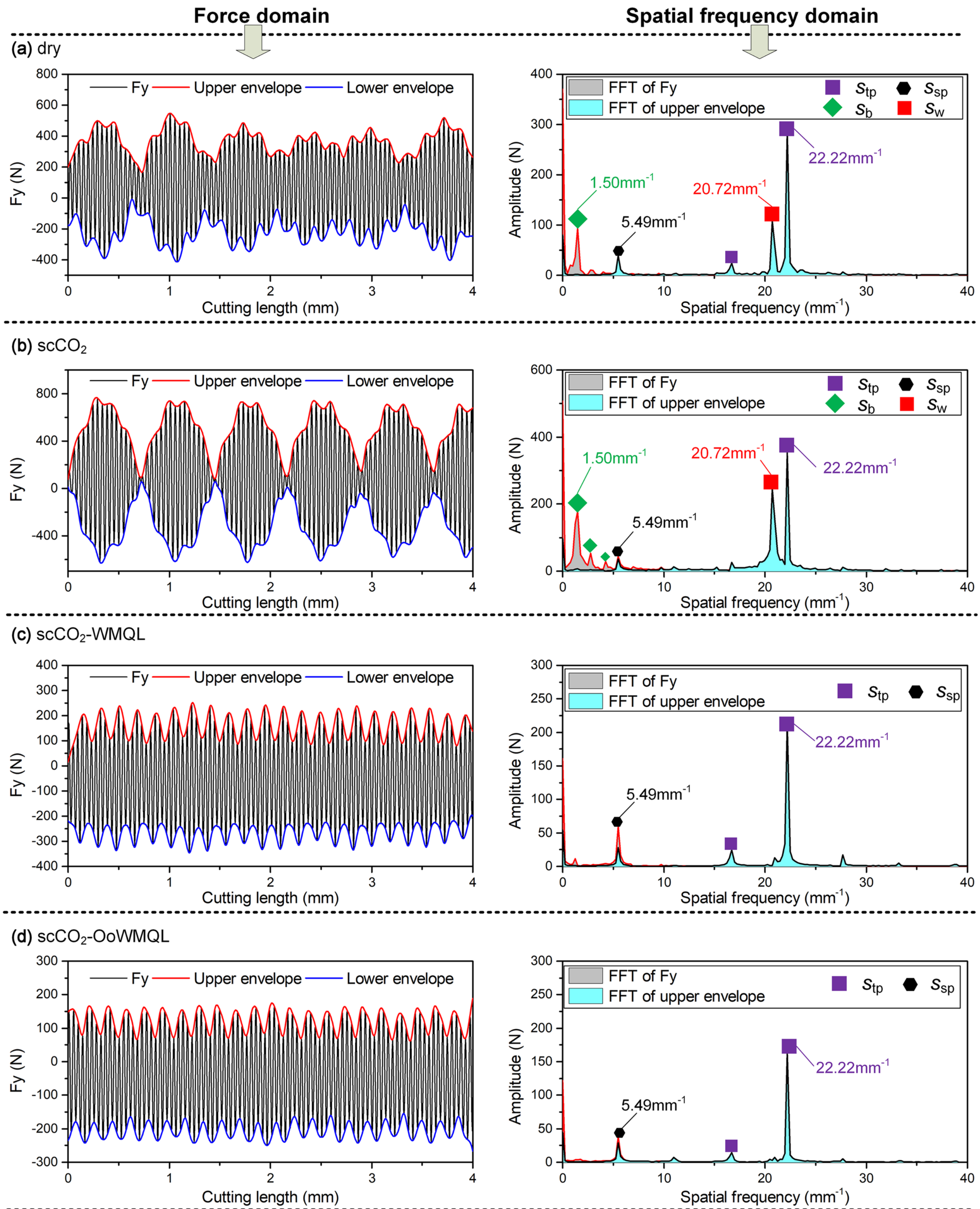

Fig. 14 Dynamic milling force in normal direction and its spectrum of experiment No. 3 **a** dry **b** $scCO_2$ **c** $scCO_2$-WMQL **d** $scCO_2$-OoWMQL

observing the spectrum of F_y. As shown in Fig. 14a, b, an excitation signal ($s_w = 20.72$ mm^{-1}) near the tooth passing frequency ($s_{tp} = 22.22^{-1}$) appears under dry and $scCO_2$ CEs, which is the cause of beat vibration. The distance between two adjacent beats of cutting force is approximately equal to the mean width of the profile elements *RSm* (Fig. 13a, b). The fundamental frequency (in spatial frequency domain) of upper envelope of cutting force that is also called beat frequency is 1.50 mm^{-1}, which is approximately equal to that of machined surface profile (Fig. 13a, b). No beat vibration occurs in milling process under $scCO_2$-WMQL and $scCO_2$-OoWMQL CEs, spectrum of F_y has only two distinct tooth passing frequency s_{tp} (22.22 mm^{-1}) and spindle frequency s_{sp} (5.49 mm^{-1}). The distance between two adjacent peaks of the milling force envelope is $4f_z$, and the fundamental frequency of upper envelope is equal to s_{sp}, which is caused by radial run-out of tool.

4 Conclusion

The present article investigates the cutting force and its coefficients, cutting temperature, surface roughness, surface morphology and beat vibration phenomenon in peripheral milling of Ti-6Al-4V under various cutting parameters and four green CEs (dry, $scCO_2$, $scCO_2$-wCMQL, $scCO_2$-OoWCMQL). The following conclusions are drawn from this study:

(1) Cutting force increases by 273.6% on average with v_c increasing from 20 to 60 m/min regardless of CEs due to formation of BUE. The lowest cutting force is obtained under $scCO_2$-OoWCMQL CE owing to its excellent cooling/lubrication, chip evacuation, chip reduction and tool-chip contact length reducing effect. Cutting force increases by 8–64% under $scCO_2$ because of the increased strength and hardness of material and deteriorated friction of tool-workpiece interface.

(2) The maximum and minimum edge force coefficients K_{te} and K_{re} are obtained for $scCO_2$-OoWMQL and $scCO_2$, respectively. OoW droplets in cryogenic $scCO_2$ significantly improve the friction of tool-workpiece interface, whereas only applying $scCO_2$ without lubricants will worsen friction. CE has a marginal effect on K_{tc}, which means that the cooling/lubrication environment does not change the shearing of cutting layer. K_{rc} is reduced under $scCO_2$-WMQL and $scCO_2$-OoWMQL CEs, indicting the spring-back of material is inhibited

(3) Lowest cutting temperature and best surface finish are obtained under $scCO_2$-OoWCMQL CE owing to the forced convection heat transfer, vaporization, chip evacuation promoting of $scCO_2$ and lubrication of OoW particles. Cutting temperature increases with v_c, f_z and a_e. Surface roughness increase with v_c and f_z, a_e shows little influence on it.

(4) For $v_c = 60$ m/min, $f_z = 0.045$ mm/r, $a_e = 0.3$ mm, beat vibration occurs under dry and $scCO_2$, vibration waviness is left on the machined surface, the radial vibration frequency of tool is 11.94 Hz. The fundamental frequency of machined surface profile is equal to that of cutting force envelope (beat frequency, 1.5 mm^{-1}), indicting cutting force directly affects surface topography. $scCO_2$-WMQL and $scCO_2$-OoWMQL CEs can improve milling stability.

(5) From the aspects of cutting force, cutting temperature, surface quality, milling stability and cleaner production, the optimum CE for peripheral finish-milling Ti-6Al-4V is $scCO_2$-OoWMQL.

Acknowledgements The work is supported by National Key R&D Program of China (2018YFB2002200).

Compliance with Ethical Standards

Conflict of interest No conflict of interest exists for all participating authors.

References

1. An, Q., & Dang, J. (2019). Cooling effects of cold mist jet with transient heat transfer on high-speed cutting of titanium alloy. *International Journal of Precision Engineering and Manufacturing-Green Technology*. https://doi.org/10.1007/s40684-019-00076-7.
2. Li, M., Yu, T., Zhang, R., Yang, L., Li, H., & Wang, W. (2018). MQL milling of TC4 alloy by dispersing graphene into vegetable oil-based cutting fluid. *The International Journal of Advanced Manufacturing Technology, 99*(5), 1735–1753.
3. Nam, J., & Lee, S. W. (2018). Machinability of titanium alloy (Ti-6Al-4V) in environmentally-friendly micro-drilling process with nanofluid minimum quantity lubrication using nanodiamond particles. *International Journal of Precision Engineering and Manufacturing-Green Technology, 5*(1), 29–35.
4. Amiril, S. A. S., Rahim, E. A., & Syahrullail, S. (2017). A review on ionic liquids as sustainable lubricants in manufacturing and engineering: Recent research, performance, and applications. *Journal of Cleaner Production, 168*, 1571–1589.
5. Gajrani, K. K., Suvin, P. S., Kailas, S. V., & Sankar, M. R. (2019). Hard machining performance of indigenously developed green cutting fluid using flood cooling and minimum quantity cutting fluid. *Journal of Cleaner Production, 206*, 108–123.
6. Wang, C., Lin, H., Wang, X., Zheng, L., & Xiong, W. (2017). Effect of different oil-on-water cooling conditions on tool wear in turning of compacted graphite cast iron. *Journal of Cleaner Production, 148*, 477–489.
7. Krolczyk, G. M., Nieslony, P., Maruda, R. W., & Wojciechowski, S. (2017). Dry cutting effect in turning of a duplex stainless steel as a key factor in clean production. *Journal of Cleaner Production, 142*, 3343–3354.
8. Mia, M., Gupta, M. K., Lozano, J. A., Carou, D., Pimenov, D. Y., Królczyk, G., et al. (2019). Multi-objective optimization and life

cycle assessment of eco-friendly cryogenic N2 assisted turning of Ti-6Al-4V. *Journal of Cleaner Production, 210*, 121–133.
9. Bordin, A., Sartori, S., Bruschi, S., & Ghiotti, A. (2017). Experimental investigation on the feasibility of dry and cryogenic machining as sustainable strategies when turning Ti6Al4V produced by additive manufacturing. *Journal of Cleaner Production, 142*, 4142–4151.
10. Yuan, S. M., Yan, L. T., Liu, W. D., & Liu, Q. (2011). Effects of cooling air temperature on cryogenic machining of Ti-6Al-4V alloy. *Journal of Materials Processing Technology, 211*(3), 356–362.
11. Pervaiz, S., Anwar, S., Qureshi, I., & Ahmed, N. (2019). Recent advances in the machining of titanium alloys using minimum quantity lubrication (MQL) based techniques. *International Journal of Precision Engineering and Manufacturing-Green Technology, 6*(1), 133–145.
12. Bai, X., Li, C., Dong, L., & Yin, Q. (2019). Experimental evaluation of the lubrication performances of different nanofluids for minimum quantity lubrication (MQL) in milling Ti-6Al-4V. *The International Journal of Advanced Manufacturing Technology, 101*(9), 2621–2632.
13. Mia, M., Gupta, M. K., Singh, G., Królczyk, G., & Pimenov, D. Y. (2018). An approach to cleaner production for machining hardened steel using different cooling-lubrication conditions. *Journal of Cleaner Production, 187*, 1069–1081.
14. Krolczyk, G. M., Maruda, R. W., Krolczyk, J. B., Nieslony, P., Wojciechowski, S., & Legutko, S. (2018). Parametric and nonparametric description of the surface topography in the dry and MQCL cutting conditions. *Measurement, 121*, 225–239.
15. Bagherzadeh, A., & Budak, E. (2018). Investigation of machinability in turning of difficult-to-cut materials using a new cryogenic cooling approach. *Tribology International, 119*, 510–520.
16. Mia, M. (2018). Mathematical modeling and optimization of MQL assisted end milling characteristics based on RSM and Taguchi method. *Measurement, 121*, 249–260.
17. Behera, B. C., Alemayehu, H., Ghosh, S., & Rao, P. V. (2017). A comparative study of recent lubri-coolant strategies for turning of Ni-based superalloy. *Journal of Manufacturing Processes, 30*, 541–552.
18. Mia, M., & Dhar, N. R. (2018). Effects of duplex jets high-pressure coolant on machining temperature and machinability of Ti-6Al-4V superalloy. *Journal of Materials Processing Technology, 252*, 688–696.
19. Faga, M. G., Priarone, P. C., Robiglio, M., Settineri, L., & Tebaldo, V. (2017). Technological and sustainability implications of dry, near-dry, and wet turning of Ti-6Al-4V alloy. *International Journal of Precision Engineering and Manufacturing-Green Technology, 4*(2), 129–139.
20. Yuan, Y., Wang, C., Yang, J., Zheng, L., & Weiqiang, X. (2018). Performance of supercritical carbon dioxide (scCO2) mixed with oil-on-water (OoW) cooling in high-speed milling of 316L stainless steel. *Procedia CIRP, 77*, 391–396.
21. Mia, M. (2017). Multi-response optimization of end milling parameters under through-tool cryogenic cooling condition. *Measurement, 111*, 134–145.
22. Zhao, Z., & Hong, S. Y. (1992). Cooling strategies for cryogenic machining from a materials viewpoint. *Journal of Materials Engineering and Performance, 1*(5), 669–678.
23. Korkut, I., & Donertas, M. A. (2007). The influence of feed rate and cutting speed on the cutting forces, surface roughness and tool–chip contact length during face milling. *Materials and Design, 28*(1), 308–312.
24. Islam, A. K., Mia, M., & Dhar, N. R. (2017). Effects of internal cooling by cryogenic on the machinability of hardened steel. *The International Journal of Advanced Manufacturing Technology, 90*(1), 11–20.
25. Kalyan, C., & Samuel, G. L. (2015). Cutting mode analysis in high speed finish turning of AlMgSi alloy using edge chamfered PCD tools. *Journal of Materials Processing Technology, 216*, 146–159.
26. Budak, E. (2006). Analytical models for high performance milling. Part I: Cutting forces, structural deformations and tolerance integrity. *International Journal of Machine Tools and Manufacture, 46*(12), 1478–1488.
27. Budak, E., Altintaş, Y., & Armarego, E. J. A. (1996). Prediction of milling force coefficients from orthogonal cutting data. *Journal of Manufacturing Science and Engineering, 118*(2), 216–224.
28. Budak, E. (1994). Mechanics and dynamics of milling thin walled structures, Doctoral dissertation, University of British Columbia.
29. Nieslony, P., Krolczyk, G. M., Zak, K., Maruda, R. W., & Legutko, S. (2017). Comparative assessment of the mechanical and electromagnetic surfaces of explosively clad Ti–steel plates after drilling process. *Precision Engineering, 47*, 104–110.
30. Grossi, N., Scippa, A., Sallese, L., Montevecchi, F., & Campatelli, G. (2018). On the generation of chatter marks in peripheral milling: A spectral interpretation. *International Journal of Machine Tools and Manufacture, 133*, 31–46.

Publisher's Note Springer Nature remains neutral with regard to jurisdictional claims in published maps and institutional affiliations.

Chongyan Cai is a Ph.D. candidate in Shanghai Jiao Tong University. His main direction of scientific activity is modelling and improvement of manufacturing processes. His current research interests include green manufacturing, surface engineering and surface morphology modelling in high-speed machining of aerospace difficult-to-cut materials such as titanium alloy and carbon fibre reinforced plastics.

Xu Liang is a master degree candidate in Shanghai Jiao Tong University. He studies cutting and process technology through experiments and numerical methods. In addition, he focuses on green cutting technology such as supercritical CO_2, oils on water (OoW) and minimum quantity lubrication (MQL).

Qinglong An is an associate professor in Shanghai Jiao Tong University. He received his doctorate from the Nanjing University of Aeronautics and Astronautics. His research interests mainly include the high-efficiency machining of carbon fibre reinforced plastics, high-speed cutting/high-efficiency grinding theory and application, green manufacturing of the difficult-to-cut materials. He has published many academic papers in the peer-reviewed journals as the first or corresponding author, such as IJMTM, ASME-JMSE, IJPEM, Composite Structures, etc. He ever won the second prize of National Scientific and Technological Progress Award (3/10) in 2017.

Zhengrui Tao is currently pursuing an M.Sc. in Mechanical Engineering at the Shanghai Jiao Tong University. He researched on data-driven intelligent predictive maintenance, with a focus on diagnosis, prognostics, and remaining useful life prediction. Most recently, he has been working on the virtual machining system focusing on chatter stability analysis and feed rate optimization. He ever was rewarded as the National scholarship for Graduates.

Weiwei Ming is an assistant research fellow in Shanghai Jiao Tong University. He received Ph.D. from the same university. His current research interests include high-efficiency machining of aerospace difficult-to-cut materials and big data technology.

Ming Chen is a Professor, Director of Institute of Manufacturing Technology and Equipment Automation, Shanghai Jiao Tong University. He has published about 300 scientific papers and 8 books. He is a member of the International Abrasive Technology Committee, and he is also an editorial board member of some of the well-known journals. His research interests mainly include the high-efficiency machining of carbon fibre reinforced plastics, high-speed cutting/high-efficiency grinding theory and application, green manufacturing of the difficult-to-cut materials. He ever won the second prize of National Scientific and Technological Progress Award of China (1/10) in 2017.